

https://dspace.org/

EFFECT OF ACID HYDROLYSES ON PROPERTIES OF CELLULOSEPOLY FURFURAL ALCHOL PFA COMPOSITES FROM MAIZE STALK

Nduduzo Khumalo; S Mohomane; L Linganiso; Ella Linganiso; Sandile Songca ...

https://hdl.handle.net/10539/39736
WOS

Downloaded from a DSpace repository. https://dspace.org/

WOOD RESEARCH doi.org/10.37763/wr.1336-4561/68.1.96111
ISSN 1336-4561 e-ISSN 2729-8906
68(1): 2023 96-111 pp.

EFFECT OF ACID HYDROLYSES ON PROPERTIES OF CELLULOSE/POLY FURFURAL ALCOHOL (PFA) COMPOSITES FROM MAIZE STALK

NDUDUZO KHUMALO, MASULUBANYE S. MOHOMANE
UNIVERSITY OF ZULULAND (KWADLANGEZWA CAMPUS)
SOUTH AFRICA

LINDA Z. LINGANISO
DURBAN UNIVERSITY OF TECHNOLOGY
SOUTH AFRICA

CEBISA E. LINGANISO
UNIVERSITY OF THE WITWATERSRAND
SOUTH AFRICA

SANDILE SONGCA
UNIVERSITY OF KWAZULU-NATAL

MOTAUNG E. TSHWAFO[1,2]
[1]UNIVERSITY OF SOUTH AFRICA
[2]SEFAKO MAKGATHO HEALTH SCIENCE UNIVERSITY
SOUTH AFRICA

(RECEIVED JUNE 2022)

ABSTRACT

The study investigated morphology and thermal properties of cellulose/poly furfural alcohol (PFA) composites prepared from maize stalk through acid mixtures. The cellulose nanocrystals (CNCs) were extracted from maize stalk via acid hydrolysis using mixtures of various acids. The prepared CNCs were encapsulated in a PFA matrix via in situ polymerization process using *p*-toluene sulfonic acid as catalyst. The properties of untreated maize stalk, cellulose and their nanocomposites were analysed by scanning electron microscope (SEM), X-ray diffraction (XRD), Fourier transmission infrared (FTIR) and thermogravimetric analysis (TGA). The crystallinity of maize stalk was generally increased after an acid hydrolysis dominated by H_2SO_4/HNO_3 and H_2SO_4/HCl. The same trend was observed from TGA, except that

H_2SO_4/H_3PO_4 and $H_2SO_4/HClO_4$ dominated thermal stability trailed by H_2SO_4 hydrolysed CNC nanocomposite. The surface breakage of fibers observed in SEM images was depended on the strength of acids used to hydrolysed the CNC. There was also evidence of aggregation and cracked PFA surface with addition of acid hydrolysed CNCs, dependent on the acids strength. The $H_2SO_4/HClO_4$ hydrolysed CNC/PFA displayed a fairly good dispersion of CNCs in the PFA matrix with no surface breakage.

KEYWORDS: Maize stalk, cellulose, nanocrystals, poly(furfural alcohol), nanocomposites.

INTRODUCTION

Lately, the production of biodegradable materials from renewable resources has gained increase interest in preserving fossil resources. Natural fibres such as nanocellulose are interesting bio-based materials for many researchers worldwide due to properties such as low density, low cost and eco-friendliness (Kalia et al. 2013, Wang et al. 2009, Ahmad et al. 2013). In fact, nanocellulose has substantial attention in polymer composite materials because of their excellent properties that include non-toxicity and high surface area amongst others (Hu et al. 2015, Kunaver et al. 2016, Lefatshe et al. 2017, Houdellier et al. 2012, Lani et al. 2014, Laetitia et al. 2017, Candido et al. 2017). Cellulose nanocrystals (CNCs) can be extracted by using different methods such as acid hydrolysis, enzymatic hydrolysis and mechanical treatment. However, acid hydrolysis using sulphuric acid remains the widely used method as it requires shorter time and produces stable suspension with high yield and crystallinity. Moreover, it also provides good dispersion as a stable colloid system due to the esterification of hydroxyl group by sulphate ions (Yang et al. 2017, Pan et al. 2013, Kandhola et al. 2020). However, there are several disadvantages associated with the usage of sulphuric acid, namely equipment corrosion, low thermal stability of CNCs, large amounts of salt to be disposed amongst others, which limit its usage and applications (Pandi et al. 2021, Ji et al. 2019, Chazeau et al.1999, Dufresne et al. 1999, Luo et al. 2003 Terech et al. 1999, Alexandre et al. 2000). Other acids such as hydrochloric acid, acetic acid, maleic acid, nitric acid, phosphoric acid and hydrobromic acid have also been reported in the literature (González et al. 2020, Ghafary et al. 2019, AbdHamid et al. 2016, Souza et al. 2017). Nonetheless, these acids promote aggregation in most polymers and solvents due to the inter- and intra-molecular hydrogen bonding interaction formed by the abundance of surface hydroxyl groups. Of interest amongst other polymers, is brittleness and biocompatibility of poly furfural alcohol (PFA). PFA is a cross-linked thermosetting polymer produced through a mineral, organic or Lewis acid-catalysed polymerisation of furfural alcohol. It is comparable to a phenolic resin, but without the toxicity of phenol and formaldehyde compounds. It is used in applications requiring low smoke release, high flame retardancy and char yield. Moreover, it is useful in a number of fields including moulds, corrosion resistant coatings, polymer concrete, metal-casting cores, sand consolidation as well as wood adhesives and binders amongst others (González et al. 2020, Ghafary et al. 2019, AbdHamid et al. 2016, Souza et al. 2017, Nazrin et al. 2020).

There are few studies that have been reported on cellulose/poly furfural alcohol nanocomposite in the literature. Ahmed et al. (2013) reported an increased thermal properties and enhanced storage modulus of PFA nanocomposites respectively, as compared to pure PFA. The CNCs used in the study were prepared via acid hydrolysis using sisal whiskers. Motaung et al. (2016) also observed an increased thermal stability and mechanical properties when treated cellulose was blended into PFA matrix. The increase was more pronounced for composites materials predominantly prepared at temperatures above 70°C. The similar trend in thermal stability was also observed by Pranger et al. (2012). Moreover, there was a significant increase in the storage modulus of the PFA nanocomposite at low filler content related to the strong reinforcement effect of a well dispersed high-specific surface nanofiller in FA during the sonication step. Similar results in terms of thermal and mechanical properties were also reported in another study (Motaung et al. 2017). The authors reported an improvement in mechanical and thermal properties when 30% acid hydrolysis was used as compared to 50%.

None whatsoever, to the best of our knowledge, investigated effects of hydrolysis by different mixture of acids on the properties of PFA nanocomposites which is the core of the current study. Morphological and thermal properties were studied to better understand the effect of varying acid mixtures during hydrolysis on the properties of cellulose/PFA nanocomposite.

MATERIALS AND METHODS

Materials

Maize stalk waste was collected from a local farm around Empangeni, South Africa. $NaClO_2$ (98%), NaOH pellet (99.9%), HCl (32%), H_3PO_4 (85%), H_2SO_4 (98%), HNO_3 (55%), $HClO_4$ (65%) and *p*-toulenesulfonic acid monohydrate were purchased from Laboratory Suppliers, South Africa. Furfural alcohol was obtained from Illovo Sugar (South Africa) Limited Downstream Products Sezela KwaZulu-Natal.

Extraction of cellulose

The maize stalks were mechanically grounded and sieved using a Fritsch cutting mill pulveriser 15, before they were washed with distilled water and dried at 100°C for 4 hours. The dried stalks were chemically treated with 4% NaOH at 80°C for 1 hour, the process was repeated 4 times. The alkali treated maize stalk was then bleached in a buffer solution for an hour at 80°C; this step was repeated 4 times. Finally, the bleached cellulose was filtered, washed with distilled water until a neutral pH was reached and dried overnight at 50°C.

Extraction of cellulose nanocrystals

The bleached cellulose extracted above was finely crushed in a Fritsch cutting mill pulveriser 15 at 0.5mm sieve. A finely dry mass of 15 g bleached cellulose was weighed in 5 different 600 ml beakers. The following mixture of acids with concentration of 55% were prepared: H_2SO_4, H_2SO_4/HCl, H_2SO_4/HNO_3, H_2SO_4/H_3PO_4 and $H_2SO_4/HClO_4$. A volume of 250 ml of 55% H_2SO_4 was added to a beaker in an ice bath of 10°C and stirred with a mechanical stirrer for 30

min. The reaction was then quenched with distilled water and left overnight. The mixture was then subjected to a centrifuge for 15 min. Next, dialysis against distilled water was performed for 5 days until pH was 7. Finally, the nanocrystals were then dried in an oven over 5 days at 30°C. The same procedure was repeated for other acid mixtures (Ahmad et al. 2013, Motaung et al. 2016, 2017).

Preparation of cellulose PFA nanocomposites

A mass of 0.6 g of *p*-toulenesulfonic acid monohydrate was dissolved in 10 ml of distilled water. The prepared catalyst was added drop-wise with continuous stirring to 200 ml furfural alcohol (FA). The acid catalysed FA was then slowly added to the cellulose nanocrystals. The mixture was then left at room temperature undisturbed overnight until it solidified. The solidified mixture was then kept at 50°C for 5 days without any disturbance to allow FA to polymerize. This was followed by curing step by further drying the mixture at 100°C for an hour. After an hour, the temperature was further increased to 160°C to achieve the desired degree of polymerization. The composites were then cooled down to room temperature.

Fourier transform infrared analysis

Fourier transform infra-red (FTIR) analysis of samples were performed using a Perkin Elmer attenuated total reflection FTIR spectrometer (Perkin Elmer UATR Two) operated in the diffuse reflectance mode. The spectral region between 4000 and 500 cm^{-1} was used during sample analysis.

X-ray diffraction

The X-ray diffraction (XRD) samples were characterized on a Bruker AXS Advance D8 diffractometer, Karsruhe, Germany equipped with monochromatic Cu Kα (λ = 1.5406 Å) as X-ray source operating at 40 kV and 40 mA at room temperature. The crystallinity index (CI) was computed using both the Segal empirical method and deconvolution method. The Segal empirical method is calculated from the height of I_{002} and the height of I_{min} between the 002 peak and the 001 peak. The CI was calculated using the method below Park et al. (2010):

$$CI\ \% = \frac{I_{002} - I_{am}}{I_{002}} \times 100 \quad (1)$$

where: I_{002} denotes the maximum intensity of diffraction of the 002 peak, while I_{am} denotes the intensity of diffraction of the amorphous material (Park et al. 2010).

Using the deconvolution method, the CI is determined using the ratio of the area of all crystalline peaks to the total area:

$$CI\ \% = \frac{\Sigma A_{cryst}}{\Sigma A_{cryst} + \Sigma A_{amorp}} \times 100 \quad (2)$$

where: A_{cryst} denotes the area of crystalline domain and A_{amorp} denotes the area of the amorphous domain.

Scanning electron microscopy

The scanning electron microscopy (SEM) measurements of samples were carried out on a FEI Quanta 200 electron microscopy operated at an accelerating voltage of 20 kV. The samples were carbon-coated before the analysis using Edward's E306A coating system.

Thermogravimetric analysis

Thermogravimetric analysis (TGA) of samples was conducted using TGA analyser (Perkin Elmer Pyris 6). Samples ranging from 10-15 mg were heated at a temperature range 35 to 900°C at a heating rate of 5°C per min under nitrogen environment at a flow rate of 20 $ml \cdot min^{-1}$.

RESULTS AND DISCUSSION

Fourier transmission infrared analysis

The FTIR spectra of untreated maize stalk, extracted cellulose and various acid hydrolysed CNCs are presented in Fig. 1. The untreated maize stalk showed characteristic behaviour of natural fibers with peaks observed at 3308 cm^{-1} (—OH stretching), 2902 cm^{-1} (C—H vibrations), 1618 cm^{-1} (C=C aromatic vibration), 1359 cm^{-1} (—CH_2 bending), 1035 cm^{-1} (C—O stretching) and 851 cm^{-1} (Kalia et al. 2013, Wang et al. 2009, Ahmad et al. 2013, Hu et al. 2015, Kunaver et al. 2016, Lani et al. 2014). There was a noticeable absence of CH_2 bending and C—O stretching for extracted cellulose, normally attributed to the removal of non-cellulosic materials (Motaung et al. 2016, 2017). After acid hydrolysis, all cellulosic characteristic peaks were observed for sulphuric acid and different mixture of acids with an additional peak at 1314 cm^{-1}, attributed to the C—H wagging of hydrogen bond. There was a notable absence of C=O stretching peak at 1737 cm^{-1} for $H_2SO_4/HClO_4$ hydrolysed CNC as compared to other acid hydrolysed cellulose. Similar to untreated maize stalk, there was a doublet peaks observed at 2902 cm^{-1} (C—H stretching of methyl group) and 2843 cm^{-1} (C—H stretching of methylene group) for H_2SO_4/H_3PO_4 hydrolysed CNC. The doublet peaks can be attributed to H_3PO_4 being a weak acid not strong enough to react with the methylene group of the cellulose.

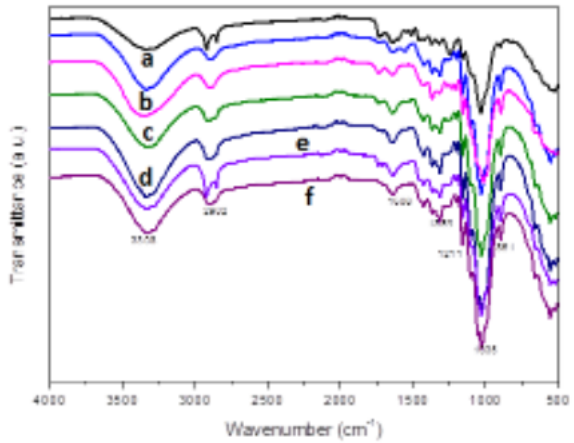


Fig. 1: FTIR spectra of (a) untreated maize stalk, (b) H_2SO_4 hydrolysed CNC, (c) H_2SO_4/HCl hydrolysed CNC, (d) H_2SO_4/HNO_3 hydrolysed CNC, (e) H_2SO_4/H_3PO_4 hydrolysed CNC and (f) H_2SO_4/$HClO_4$ hydrolysed CNC.

FTIR spectra of pure PFA and various acid hydrolysed CNCs/PFA nanocomposites are shown in Fig. 2. As usual, the FTIR spectrum of pure PFA displayed main absorption peaks at 2934, 1997 and 1380 cm^{-1} that represent the presence of the aliphatic functional groups (Ahmad et al. 2013, Motaung et al. 2016, 2017). The stretching vibration of –OH end groups was observed at around 3427 cm^{-1}. Furthermore, there was a noticeable appearance and a gradual increase in the intensity of the new peak at 1267 cm^{-1} for all various PFA nanocomposites. It was also noted that there was diminishing of stretching vibration of the OH- for H_2SO_4/HCl and H_2SO_4/HNO_3 hydrolysed CNCs/PFA nanocomposite. In fact, after encapsulation of various CNCs into the polymer matrix the absorption peaks at 2973 and 2851 cm^{-1} (C-H stretching of methyl and methylene groups respectively) emerged due to the presence of furan rings (Motaung et al. 2016). Clearly, there were three new peaks at 1420, 1355 cm^{-1} (C-H and C-O bending vibration of hydroxyl respectively) and 855 cm^{-1} (O-H bending vibration of hydroxyl) for all PFA nanocomposites. There was a noticeable similar peaks pattern for H_2SO_4/H_3PO_4 and H_2SO_4 hydrolysed CNCs/PFA nanocomposites. A close look indicated another similarity pattern between H_2SO_4/$HClO_4$ and H_2SO_4/HNO_3 hydrolysed CNCs/PFA nanocomposites. While other researchers attributed the observations to the interfacial interaction (Motaung et al. 2016, 2017) but/in addition, the current study has vehemently suggested that the new peaks could be due to the polymerization of FA to PFA which initiated the exfoliation process as it is typically convoyed by a substantial increase of the peak intensity allocated to the skeletal vibration of the 2,5-disubstituated furan rings.

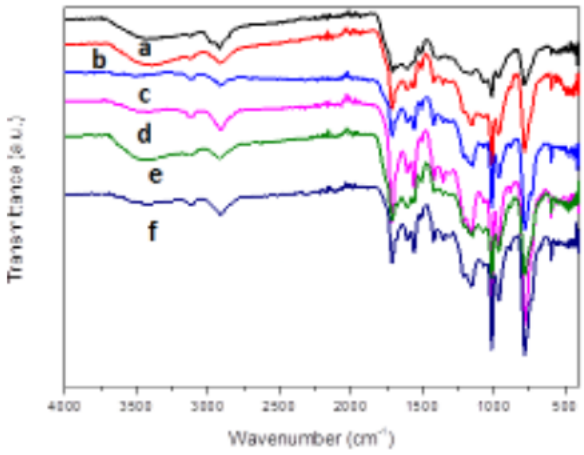


Fig. 2: FTIR spectra of (a) PFA, (b) H_2SO_4 hydrolysed CNC/PFA, (c) H_2SO_4/HCl hydrolysed CNC/PFA, (d) H_2SO_4/HNO_3 hydrolysed CNC/PFA, (e) H_2SO_4/H_3PO_4 hydrolysed CNC/PFA and (f) H_2SO_4/$HClO_4$ hydrolysed CNC/PFA.

X-*ray* diffraction analysis

XRD spectra of untreated maize stalk, extracted cellulose as well as acid hydrolysed CNCs are shown in Fig. 3. All samples displayed similar diffraction patterns at 2θ = 15, 23 and 35°, typical of lignocellulosic material (Park et al. 2010). It is clear that the intensity of the diffraction peak increased after treatments for all the samples. Of course, that is due to the removal of non-cellulosic materials such as hemicellulose and lignin as confirmed by absence of CH_2 bending and C—O stretching for extracted cellulose from FTIR. Crystallinity index (CI) values calculated using Segal empirical method and deconvolution methods are shown in Tab. 1.

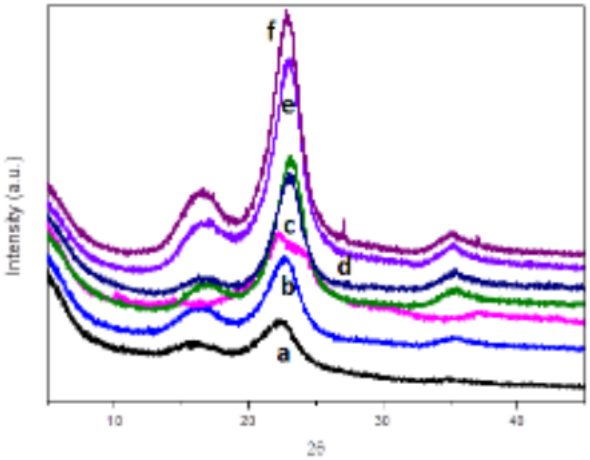


Fig. 3. XRD spectra of (a) untreated maize stalk, (b) H_2SO_4 hydrolysed CNC, (c) H_2SO_4/HCl hydrolysed CNC, (d) H_2SO_4/HNO_3 hydrolysed CNC, (e) H_2SO_4/H_3PO_4 hydrolysed CNC and (f) H_2SO_4/$HClO_4$ hydrolysed CNC.

Tab. 1: Crystalline index values of materials studied using Segal and deconvolution methods.

Fiber type	**CI (%) (Segal)**	**CI (%) (Deconvolution)**
Maize stalk untreated	32	30
Extracted cellulose	61	63

H_2SO_4 CNC	76	67
H_2SO_4/HCl CNC	83	74
H_2SO_4/HNO_3 CNC	86	77
H_2SO_4/ H_3PO_4 CNC	76	67
H_2SO_4 /$HClO_4$ CNC	61	57

There was a notable increase in CI values for all the samples as compared to untreated maize stalk. That further emphasised the removal of noncellulosic components as discussed in FTIR. H_2SO_4/HNO_3 is dominant trailed by H_2SO_4/HCl. H_2SO_4/H_3PO_4 hydrolysed CNC and H_2SO_4 hydrolysed CNC appears to have similar CI as confirmed by both Segal and deconvolution method. In addition, H_2SO_4/$HClO_4$ exhibited the lowest CI compared to the rest. The observation is attributed to the different strengths of the acid mixtures on the efficiency of noncellulosic material removal. For instance, both acid blends of the strong HCL and HNO_3 exhibited superior CI values compared to the blend of the weak H_3PO_4.

XRD patterns of pure PFA and acid hydrolysed CNC/PFA nanocomposites are shown in Fig. 4. The diffraction pattern of PFA sample showed a single peak at $2\theta = 23°$, which is a similar pattern reported by Lanchis et al. (2015). Similar diffraction pattern was also observed for all nanocomposite, with the exception of H_2SO_4/H_3PO_4 and H_2SO_4 /$HClO_4$ hydrolysed CNC/PFA nanocomposites respectively. There is no doubt from the literature that peaks for all composites indicated successful compounding of PFA composites (Luo et al. 2003, Motaung et al. 2017). The CI values were calculated using the deconvolution method and Segal method as shown in Tab. 2. It was generally clear from the XRD data, according to the methods, that PFA possesses the highest crystallinity than all nanocomposites. The order of crystallinity was reduced with the strength of the acidic medium used. The order of crystallinity was obtained as follows: pure PFA > H_2SO_4 CNC/PFA > H_2SO_4/HCl CNC/PFA > H_2SO_4/HNO_3 CNC/PFA. Both H_2SO_4/ H_3PO_4 CNC/PFA and H_2SO_4 /$HClO_4$ CNC/PFA pattern did not display any peak. It is apparent from both methods that the encapsulation of the crystalline CNCs, collapse the resulted crystalline regions in an amorphous cellulose PFA nanocomposites. Taking FTIR results into consideration, it is possible to relate the observation to the emergence of C-H stretching of methyl and methylene groups due to furfural ring interaction with cellulose.

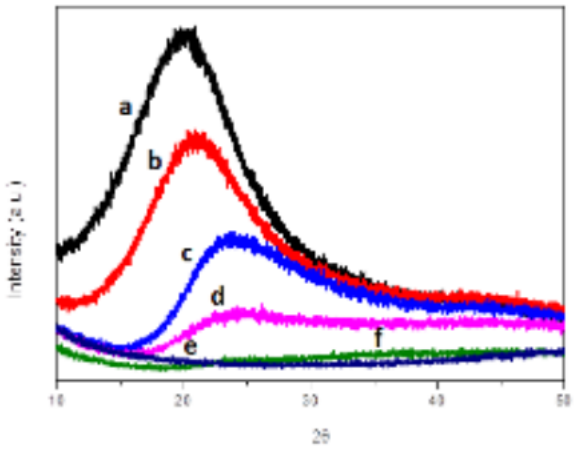


Fig. 4: XRD spectra of (a) PFA, (b) H_2SO_4 hydrolysed CNC/PFA, (c) H_2SO_4/HCl hydrolysed CNC/PFA, (d) H_2SO_4/HNO_3 hydrolysed CNC/PFA, (e) H_2SO_4/H_3PO_4 hydrolysed CNC/PFA and (f) H_2SO_4/$HClO_4$ hydrolysed CNC/PFA.

Tab. 2: Crystalline index values of cellulose (PFA) nanocomposites studied using deconvolution methods.

Fiber type	**CI (%) (deconvolution)**	**CI (%) (Segal)**
PFA	75	61
H_2SO_4 hydrolysed CNC/PFA	67	56
H_2SO_4/HCl hydrolysed CNC/PFA	46	49
H_2SO_4/HNO_3 hydrolysed CNC/PFA	26	32
H_2SO_4/H_3PO_4 hydrolysed CNC/PFA	-	-
H_2SO_4 /$HClO_4$ hydrolysed CNC/PFA	-	-

Scanning electron microscope

The SEM images of untreated maize stalk, cellulose and acid hydrolysed CNCs are presented in Fig. 5. Waxes and pectin were plainly noticed on the surface in the form of dispersed particles (Fig. 5a) which were absent after hydrolysis (Fig. 5b). Generally, the treatments reduced fibre size from approximately 60µm (untreated) to an average of 10 µm. It is also worth noting that H_2SO_4 and H_2SO_4/HNO_3 hydrolysed CNC seems to have maintained its rod like structure compared to the rest that appeared a bit deformed (see arrows). In fact, both H_2SO_4/HCl and H_2SO_4/HNO_3 hydrolysed CNCs displayed obvious characters of fibre breakage on the surface. The explanation may not be less than the strength of the acids, as they are considered strong (Abd Hamid et al. 2016, Ji et al. 2019).

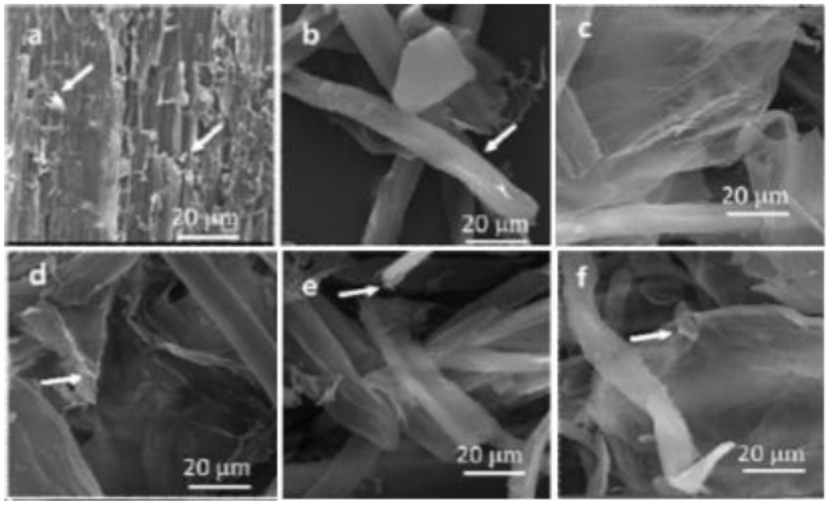


Fig. 5. SEM images of (a) untreated maize stalk, (b) H_2SO_4 hydrolysed CNC, (c) H_2SO_4/HCl hydrolysed CNC, (d) H_2SO_4/HNO_3 hydrolysed CNC, (e) H_2SO_4/H_3PO_4 hydrolysed CNC and (f) $H_2SO_4/HClO_4$ hydrolysed CNC.

The SEM images of hydrolysed CNC/PFA and various acid mixture hydrolysed CNC/PFA are presented in Fig. 6. The composites generally showed trapped fibres with others obviously broken and dispersed on the surface. Some, (Figs. 6b and 6e), indicated cavities that are arguably fairly dispersed. This suggests that some of cellulose derivatives, which are (Figs. 6c,d and 6f) in this study, generate little or no gas whatsoever during the polymerization of PFA. Despite some cavities formed in Fig. 6b, there is a clear fibres which protruded on the surface, trapped and broken (see arrows). The same observation is also noted at e, however in that case most fibres appeared trapped either inside a cavity or adjacent. Furthermore, both c and d hydrolysed nanocomposites displayed loose fibres embedded in cracks during sample preparation.

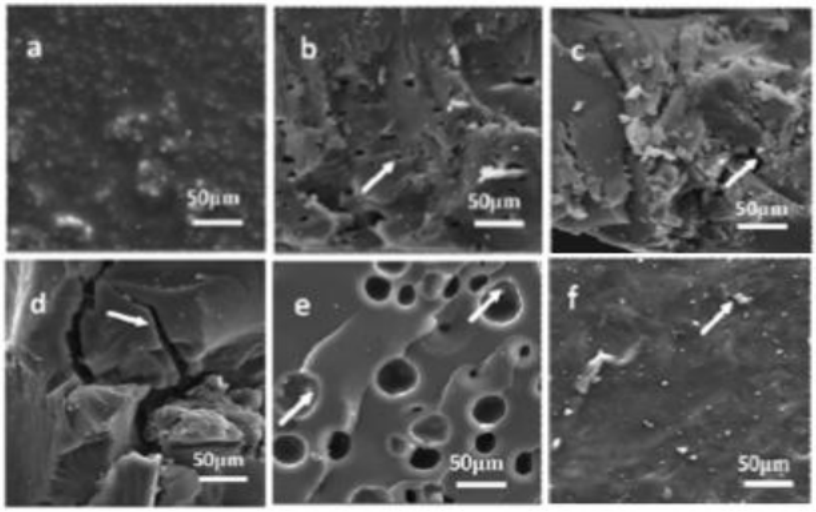


Fig. 6: SEM images of (a) PFA, (b) H_2SO_4 hydrolysed CNC/PFA, (c) H_2SO_4/HCl hydrolysed CNC/PFA, (d) H_2SO_4/HNO_3 hydrolysed CNC/PFA, (e) H_2SO_4/H_3PO_4 hydrolysed CNC/PFA and (f) $H_2SO_4/HClO_4$ hydrolysed CNC/PFA.

Thermogravimetric analysis

Thermogravimetric analysis studies were conducted to investigate the changes in thermal properties of extracted cellulose and mixture of acids hydrolysed cellulose. The TGA and DTG curves are shown in Figs. 7a,b. The cellulose spectra display two degradation steps as confirmed by the DTG curve. The first degradation step was attributed to hemicellulose, waxes and pectin while the second step to lignin degradation (Motaung et al. 2016, 2017). All the acids hydrolysed CNCs displayed one degradation step between 445°C to 460°C. There was a notable increase in thermal stability of the acids hydrolysed CNCs compared to extracted cellulose. The observed increase can be attributed to the further removal of hemicellulose, waxes and pectin from the cellulose during acid hydrolysis, as these components are known to have lower thermal stability compared to pure cellulose (Park et al. 2010). The order of thermal stability was as follows: extracted cellulose < H_2SO_4 hydrolysed CNC < H_2SO_4/HCl hydrolysed CNC < H_2SO_4/HNO_3 hydrolysed CNC < H_2SO_4/H_3PO_4 hydrolysed CNC <H_2SO_4/$HClO_4$ hydrolysed CNC. Extracted cellulose has lower thermal stability due to lignin and other amorphous regions which degrade at low temperature. The acid strength might be responsible for both H_2SO_4/HCl hydrolysed CNC and H_2SO_4/HNO_3 hydrolysed CNC as they differ by two degrees, the strong acid content could initiate a partial degradation which could result into lower thermal stability. Both H_2SO_4/H_3PO_4 and H_2SO_4/$HClO_4$ hydrolysed CNC showed the highest thermal stability due to the weak acid nature of H_3PO_4 and "moderate" acid nature of $HClO_4$.

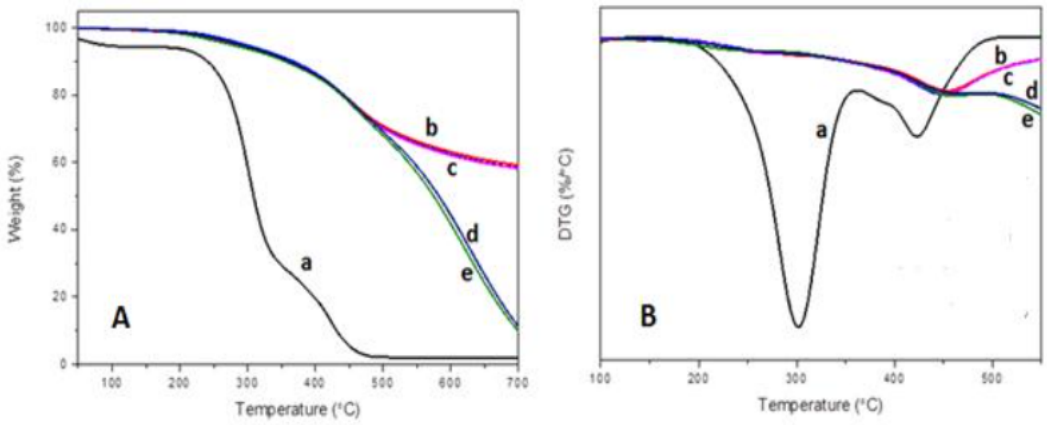


Fig. 7: TGA(A) and DTG(B) of (a) untreated maize stalk, (b) H_2SO_4 hydrolysed CNC, (c) H_2SO_4/HCl hydrolysed CNC, (d) H_2SO_4/HNO_3 hydrolysed CNC, (e) H_2SO_4/H_3PO_4 hydrolysed CNC and (f) H_2SO_4/$HClO_4$ hydrolysed CNC.

Furthermore, TGA was employed to study the effect of encapsulation of acids hydrolysed CNCs has on the thermal properties of the PFA. The TGA and DTG curves are shown in Figs. 8a,b, respectively. Pure PFA displayed two decomposition steps with the first decomposition step observed around 460°C and the second decomposition step around 644°C. These degradation steps are due to the removal of oxygen atoms and the alteration of furan rings into a condensed aromatic ring. The H_2SO_4 acid hydrolysed PFA nanocomposite also displayed two degradation steps. The first degradation step was observed around 225°C associated to scission of both methyne and methylene links. The second degradation step at high temperature

360°C was attributed to the scission of furanic links to form ketonic volatile compounds (Ahmad et al. 2013). All the mixture of acids hydrolysed CNCs nanocomposites displayed one degradation step (between 330 and 355°C) compared two degradation steps for both pure PFA and H_2SO_4 hydrolysed CNC nanocomposite. It can be noted that H_2SO_4 hydrolysed CNC nanocomposite showed a lower thermal stability than the rest. This could be due to the formation of strong intra- and inter-molecular hydrogen interaction resulted from the aggregation due to the abundance of surface hydroxyl groups. The order of thermal stability was H_2SO_4 hydrolysed nanocomposite < H_2SO_4/HCl hydrolysed nanocomposite < H_2SO_4/HNO_3 hydrolysed nanocomposite < H_2SO_4/$HClO_4$ hydrolysed nanocomposite < H_2SO_4/H_3PO_4 nanocomposite < pure PFA. The order is similar to the order observed for CNCs and follows the order of acid strength.

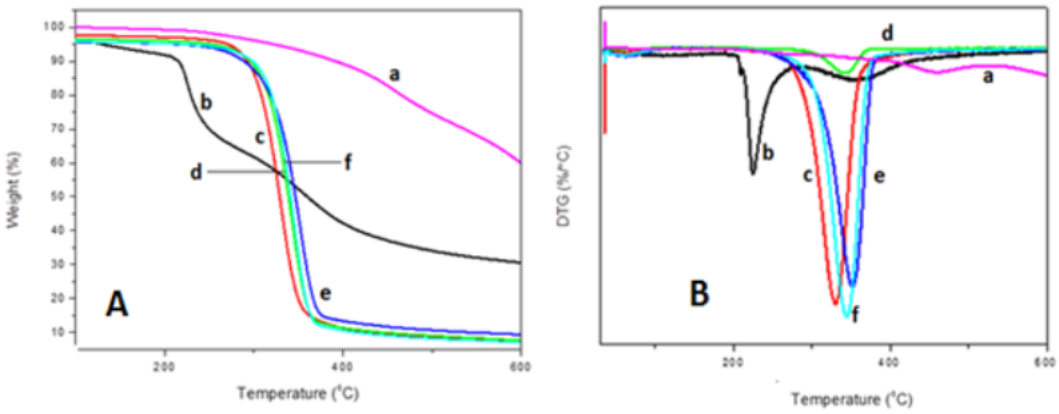


Fig. 8: TGA(A) and DTG(B) of (a) PFA, (b) H_2SO_4 hydrolysed CNC/PFA, (c) H_2SO_4/HCl hydrolysed CNC/PFA, (d) H_2SO_4/HNO_3 hydrolysed CNC/PFA, (e) H_2SO_4/H_3PO_4 hydrolysed CNC/PFA and (f) H_2SO_4/$HClO_4$ hydrolysed CNC/PFA.

CONCLUSIONS

The main objective of the study was to investigate the effect of acid mixtures on crystallinity, thermal and morphological properties of the resultant CNC/PFA nanocomposites. As expected, there was an increase in crystallinity when extracted cellulose was treated with acid hydrolysis using sulphuric acid as well as mixture of acids. The highest CI were observed for strong acids i.e. H_2SO_4, HNO_3 and HCl. The incooperation of various acids hydrolysed CNC in PFA matrix attenuated the crystallinity index of the resultant nanocomposites. It is also known that the usage of sulphuric acid often resultant in low thermal stability of CNCs, which affected the thermal stability of PFA matrix. The H_2SO_4 hydrolysed CNC nanocomposite exhibited a lower thermal stability than the rest of the nanocomposites. However, there was an improvement with the addition of the second acid with thermal stability depended on the acidic strength. The SEM images echoed both the TGA and crystallinity studies, results with broken trapped fibres and fibre pull-out observed for mixtures using strong acids, i.e. H_2SO_4, HNO_3 and HCl. For mild and moderate acids such as $HClO_4$, the SEM image of H_2SO_4/$HClO_4$ hydrolysed CNC/PFA displayed a fairly good dispersion of CNCs in the PFA matrix with little surface breakages.

REFERENCES

1. AbdHamid, S.B., Zain, S.K., Das, R., Centi, G., 2016: Synergic effect of tungstophosphoric acid and sonication for rapid synthesis of crystalline nanocellulose. Carbohydrate polymers 138: 349-355.
2. Abidi, N., Hequet, E., Cabrales, L., 2011: Applications of Fourier transform infrared spectroscopy to study cotton fibers. Fourier transforms - new analytical approaches and FTIR strategies: 89-114.
3. Ahmad, E., Luyt, A., Djoković, V., 2013: Thermal and dynamic mechanical properties of bio-based poly (furfuryl alcohol)/sisal whiskers nanocomposites. Polymer bulletin 70(4): 1265-1276.
4. Alexandre, M., Dubois, P., 2000: Polymer-layered silicate nanocomposites: preparation, properties and uses of a new class of materials. Materials science and engineering: R: Reports 28(1-2): 1-63.
5. Candido, R., Godoy, G., Goncalves, A.R., 2017: Characterization and application of cellulose acetate synthesized from sugarcane bagasse. Carbohydrate Polymers 167: 280-289.
6. Chazeau, L., Cavaillé, J.Y., Canova G., Dendievel R., Boutherin B., 1999: Viscoelastic properties of plasticized PVC reinforced with cellulose whiskers. Journal of Applied Polymer Science 71(11): 1797-1808.
7. Couret L., Irle M., Belloncle C., Cathala B., 2017: Extraction and characterization of cellulose nanocrystals from post-consumer wood fiberboard waste. Cellulose 24: 2125-2137.
8. doNascimento, D.M., Almeida, J.S., Vale., M., Leitão, R.C., Muniz, R.C., deFigueirêdo, M.C., Morais, J.P.S., Rosa M.F., 2016: A comprehensive approach for obtaining cellulose nanocrystal from coconut fiber. Part I: Proposition of technological pathways. Industrial Crops and Products 93: 66-75.
9. Dufresne, A., Kellerhals, M.B., Witholt, B., 1999: Transcrystallization in MCl-PHAs/cellulose whiskers composites. Macromolecules 32(22): 796-7401.
10. Ghafary, S., Ranjbar, S., Larijani B., Amini, M., Biglar, M., Mahdavi, M., Bakhshaei M., Khoshneviszadeh, M., Sakhteman, A., Khoshneviszade, M., 2019: Novel morpholine containing cinnamoyl amides as potent tyrosinase inhibitors. International journal of biological macromolecules 135: 978-985.
11. González, M.M., Blanco-Tirado, C. Combariza, M.Y., 2020: Nanocellulose as an inhibitor of water-in-crude oil emulsion formation. Fuel 264: 116830.
12. Houndellier, F., Masseboeuf, A., Monthhioux, M., Hÿtch, M.j., 2012: New carbon cone nanotip for use in a highly coherent cold field emission electron microscope. Carbon 50(5): 2037-2044.
13. Hu, F., Lin, N., Chang, P.R., Huang, J., 2015: Reinforcement and nucleation of acetylated cellulose nanocrystals in foamed polyester composites. Carbohydrate Polymers 129: 208-215.

14. Ji, H., Xiang, Z., Qi, H., Han, T., Pranovich, A., Song, T., 2019: Strategy towards one-step preparation of carboxylic cellulose nanocrystals and nanofibrils with high yield, carboxylation and highly stable dispersibility using innocuous citric acid. Green Chemistry 21(8): 1956-1964.
15. Kalai, S., Thakur, K., Celli, A., Kiechel, M.A., Schauer, L.C., 2013: Surface modification of plant fibers using environment friendly methods for their application in polymer composites, textile industry and antimicrobial activities: A review. Journal of Environmental Chemical Engineering 1(3): 97-112.
16. Kandhola, G., Djioleu, A., Rajan, K., Labbé, N., Sakon, J., Carrier, D.J., Kim, J.W., 2020: Maximizing production of cellulose nanocrystals and nanofibers from pre-extracted loblolly pine kraft pulp: a response surface approach. Bioresources and Bioprocessing 7(1): 1-16.
17. Kunaver, M., Anžlovar, A., Žagar., E., 2016: The fast and effective isolation of nanocellulose from selected cellulosic feedstocks. Carbohydrate polymers 148: 251-258.
18. Lanchis, R., Rosca, I.D., Ghiurea, M., Spataru, C.I., Nicolae, C.A., Gabor, R., Raditoiu, V., Preda, S., Fierascu, R.C., Donescu, D., 2015: Synthesis and properties of new epoxy-organolayered silicate nanocomposites. Applied Clay Science 103: 28-33.
19. Lani, N.S., Ngadi, N., Johari, A., Jusoh, M., 2014: Isolation, characterization, and application of nanocellulose from oil palm empty fruit bunch fiber as nanocomposites. Journal of Nanomaterials 129: 208-215.
20. Lefatshe, K., Muiva, C.M., Kebaabetswe, L.P., 2017: Extraction of nanocellulose and in-situ casting of ZnO/cellulose nanocomposite with enhanced photocatalytic and antibacterial activity. Carbohydrate Polymers 164: 301-308.
21. Luo, J.J., Daniel, I.M., 2003: Characterization and modeling of mechanical behavior of polymer/clay nanocomposites. Composites Science and Technology 63(11): 1607-1616.
22. Motaung, T.E., Gqokoma, Z., Linganiso, L.Z., Hato, M.J., 2016: The effect of acid content on the poly (furfuryl) alcohol/cellulose composites. Polymer Composites 37(8): 2434-2441.
23. Motaung, T.E., Linganiso, L.Z., Kumar, R., Anandijwala, R.D., 2017: Agave and sisal fibre-reinforced polyfurfuryl alcohol composites. Journal of Thermoplastic Composite Materials 30(10): 1323-1343.
24. Nazrin, A., Sapuan, S.M., Zuhri, M.Y.M, Ilyas, R.A., Syafiq, R., Sherwani, S.F.K., 2020: Nanocellulose reinforced thermoplastic starch (TPS), polylactic acid (PLA), and polybutylene succinate (PBS) for food packaging applications. Frontiers in Chemistry 8: 213.
25. Pan, M., Zhou, X., Chen, M., 2013: Cellulose nanowhiskers isolation and properties from acid hydrolysis combined with high pressure homogenization. BioResources 8(1): 933-943.
26. Pandi, N., Sonawane, S.H., Kishore, K.A., 2021: Synthesis of cellulose nanocrystals (CNCs) from cotton using ultrasound-assisted acid hydrolysis. Ultrasonics Sonochemistry 70: 105353.
27. Park, S., Baker, J.O., Himmel, M.E.,Parilla, P.A., Johnson, D.K., 2010: Cellulose crystallinity index: measurement techniques and their impact on interpreting cellulase performance. Biotechnology for Biofuels 3(1): 1-10.

28. Pranger, L.A., Nunnery G.A., Tannenbaum R., 2012: Mechanism of the nanoparticle-catalyzed polymerization of furfuryl alcohol and the thermal and mechanical properties of the resulting nanocomposites. Composites Part B: Engineering 43(3): 1139-1146.
29. Souza, A.G., Kano, F.S., Bonvent, J.J., Rosa, D., 2017: Cellulose nanostructures obtained from waste paper industry: a comparison of acid and mechanical isolation methods. Materials Research 20: 209-214.
30. Terech, P., Chazeau, L., Cavaille, J.A., 1999: Small-angle scattering study of cellulose whiskers in aqueous suspensions. Macromolecules 32(6): 1872-1875.
31. Wang, L., Kumar, R., Zhang, L., 2009: Investigation into hemp fiber-and whisker-reinforced soy protein composites. Frontiers of Chemistry in China 4(3): 313-320.
32. Xiong, R., Zhang, X., Tian, D., Zhou, Z., Lu, C., 2012: Comparing microcrystalline with spherical nanocrystalline cellulose from waste cotton fabrics. Cellulose 19(4): 1189-1198.
33. Yang, X., Han, F., Xu, C., Jiang, S., Huang, L., Liu, L., Xia, Z., 2017: Effects of preparation methods on the morphology and properties of nanocellulose (NC) extracted from corn husk. Industrial Crops and Products 109: 241-247.

NDUDUZO KHUMALO, MASULUBANYE S. MOHOMANE
UNIVERSITY OF ZULULAND (KWADLANGEZWA CAMPUS)
POLYMER CHEMISTRY UNIT, DEPARTMENT OF CHEMISTRY
PRIVATE BAG X1001, KWADLANGEZWA 3886
SOUTH AFRICA

LINDA Z. LINGANISO
DURBAN UNIVERSITY OF TECHNOLOGY
41/43 M L SULTAN RD, GREYVILLE, DURBAN, 4001
SOUTH AFRICA

CEBISA E. LINGANISO
UNIVERSITY OF THE WITWATERSRAND
[1]MICROSCOPY AND MICROANALYSIS UNIT
[2]SCHOOL OF CHEMISTRY
MOLECULAR SCIENCES INSTITUTE
JOHANNESBURG 2050
SOUTH AFRICA

SANDILE SONGCA
UNIVERSITY OF KWAZULU-NATAL
SCHOOL OF CHEMISTRY AND PHYSICS, UNIVERSITY OF KWAZULU NATAL,
DURBAN 4041, SOUTH AFRICA

MOTAUNG E. TSHWAFO*[1,2]
[1]UNIVERSITY OF SOUTH AFRICA
SCHOOL OF SCIENCE IN THE COLLEGE OF SCIENCE ENGINEERING AND TECHNOLOGY
DEPARTMENT OF CHEMISTRY
PO BOX 392, UNISA 0003
JOHANNESBURG 2050
SOUTH AFRICA
[2]SEFAKO MAKGATHO HEALTH SCIENCE UNIVERSITY
DEPARTMENT OF CHEMISTRY
P.O. BOX 94, MEDUNSA, 0204
SOUTH AFRICA
*Corresponding author: motaungte@live.com or motaute1@unisa.ac.za